Available online at www.sciencedirect.com
ScienceDirect
International Journal of Heat and Fluid Flow 29 (2008) 985–1000
International Journal of HEAT AND FLUID FLOW
www.elsevier.com/locate/ijhff

Active performance enhancement of spray cooling

Anna A. Pavlova [1], Kiyoshi Otani [2], Michael Amitay [3,*]

Rensselaer Polytechnic Institute, Troy, NY 12180, USA

Received 12 December 2007; received in revised form 13 February 2008; accepted 14 February 2008
Available online 2 April 2008

Abstract

The effect of synthetic (zero-net-mass-flux) jets on a water spray and on its cooling performance in the non-boiling regime was experimentally investigated. Particle Image Velocimetry and Shadowgraphy were used to evaluate the global and detailed spray characteristics, respectively, under several modes of flow control. Temperature measurements were performed to assess the effects of spray control on the heat transfer. Heat transfer improvements were achieved with flow control, compared to the baseline case, where the mode of control, together with spray properties and the distance between the spray and the hot surface play an important role in cooling enhancement.

Keywords: Spray cooling; Active flow control; Synthetic jets; Heat transfer

1. Introduction

Spray cooling is a well known, frequently used method of heat removal in many processes. It allows for phase change in high temperature, high heat flux applications, while using less cooling fluid and covering a larger area than impinging liquid jet (having the same orifice size). Spray cooling has the advantage of additional heat removal that is thought to be due to the impacting droplets and surface renewal effects, which is useful, both in boiling and non-boiling regimes. There has been a significant amount of experimental, analytical, and numerical research on sprays and spray cooling over the last several decades in order to understand the basic mechanisms of sprays and spray cooling behavior (e.g., Ghodbane and Holman, 1991; Estes and Mudawar, 1995a,b; Sirignano, 1999; Navedo, 2000; Cossali, 2001; Hardalupas and Horender, 2001; Chen et al., 2002, 2004).

Spray parameters are highly dependent on the specific spray nozzle used (Lefebvre, 1989; Pimentel et al., 2006), which makes it difficult to alter them without a complete overhaul of the system. However, it is the spray parameters (i.e., droplet size, concentration, and distribution) that are crucial for the spray cooling performance, as indicated by many authors. The addition of an effective active flow control approach that could enable manipulation of spray behavior and parameters, as necessary, would enhance the versatility and efficiency of sprays in spray cooling applications.

The effect of spray parameters on the spray's heat removal ability has been the topic of investigation for many researchers. Estes and Mudawar (1995a) experimentally compared free jets and sprays (with an FC-72 as the working fluid) in cooling a chip to investigate the effects of key parameters on cooling performance. They found that spray cooling produced much higher CHF values than jets for lower subcooling due to the better ability of spray droplets to stay in contact with the surface, resulting in delayed CHF. In their follow-up work (Estes and Mudawar, 1995b), the nucleate boiling heat transfer and CHF for full cone sprays were investigated, taking into consideration

* Corresponding author. Tel.: +1 518 276 3340.
E-mail address: amitam@rpi.edu (M. Amitay).
[1] Graduate Student, Mechanical Aerospace and Nuclear Engineering, 110 8th Street, Troy, NY.
[2] Visiting Scholar, Mechanical Aerospace and Nuclear Engineering, 110 8th Street, Troy, NY.
[3] Assistant Professor, Mechanical Aerospace and Nuclear Engineering, 110 8th Street, Troy, NY.

0142-727X/$ - see front matter © 2008 Elsevier Inc. All rights reserved.
doi:10.1016/j.ijheatfluidflow.2008.02.006

Nomenclature

A_h	area of the heater
A_j	area of the synthetic jet orifice
A_s	area of the spray nozzle orifice
C_μ	momentum coefficient, $C_\mu = \frac{nA_jU_o^2}{A_sU_e^2}$
D	diameter of the heater
d	jet orifice diameter
d_d	droplet diameter
d_s	spray nozzle orifice diameter
dt	time step
f	driving (formation) frequency of synthetic jet
g	acceleration due to gravity
H	distance between the orifice and heated surface
k	thermal conductivity
L_o	synthetic jet stroke length, $L_o = \int_0^{\tau/2} u(t)\,dt$
L_w	elevation of water intake level above nozzle orifice
N_b	number of droplets for baseline case
$N_{b\|tot}$	total number of droplets for baseline case
N_f	number of droplets with flow control
q''	heat flux
Q_a	air flow rate supplied to the spray nozzle
Q_w	water flow rate produced by the spray nozzle
R	radius of the heater
r	radial direction
Re_{U_o}	Reynolds number based on average orifice velocity, $Re_{U_o} = \frac{U_o d}{v}$
Re_{U_p}	Reynolds number based on peak velocity, $Re_{U_p} = \frac{U_p d}{v}$
S	spray
SJ	synthetic jet
St	Strouhal number, $St = \frac{f \cdot d}{U_o}$
T	temperature
t	time
T_∞	ambient temperature
T_b	temperature of baseline case
T_f	temperature with flow control
T_w	temperature of the heated surface
ΔT	temperature difference between the surface of the heater and water
U	streamwise velocity
U_{av_o}	average velocity of the continuous jet at the orifice plane
U_{CL}	centerline velocity of the spray
U_{cl}	centerline velocity at the jet exit plane
U_e	average air exit velocity at the spray orifice, $U_e = \frac{Q_a}{A_s}$
U_{max_b}	maximum centerline velocity of the spray
$U_{max\|L_{w\,max}}$	maximum centerline velocity of spray at maximum L_w
U_o	average orifice velocity; $U_o = \frac{L_o}{\tau}$
U_p	peak orifice velocity
$u(t)$	periodic centerline velocity at the jet exit plane
V	cross-stream velocity
x	streamwise coordinate
y	cross-stream coordinate
z	span-wise coordinate
Δ	change in
δ	spray width
θ	vectoring angle
τ_p	period of flapping actuation
τ	cycle period in s; $\tau = 1/f$

the effects of spray nozzle, volumetric flux, subcooling, and working fluid. They showed that dense sprays reduced evaporation efficiency, as compared to less dense sprays and found a correlation for accurate data prediction for FC-72, FC-87, and water. This correlation indicated a strong dependence of CHF on the Sauter mean diameter and volumetric flux, where CHF increases with greater subcooling and smaller drop size. The Sauter mean diameter for full cone sprays was found to depend on the orifice diameter, Weber number, and Reynolds number.

The effect of the nozzle-to-surface distance for full cone sprays was investigated by Mudawar and Estes (1996), where they showed that the optimal configuration was when the impact area of the spray just inscribed the heated area. By collecting data over a range of flow rates and subcooling regimes, the authors also developed a correlation for spray cooling of small surfaces.

An extensive parametric study on the effects of spray characteristics on spray cooling heat transfer was conducted by Navedo (2000), where each parameter was varied independently of the others for several nozzles. He found that droplet velocity had the greatest effect on CHF but did not significantly affect the heat transfer coefficient, whereas increasing the number of droplets increased both the CHF and the heat transfer coefficient. Furthermore, a decrease in the Sauter mean diameter increased the heat transfer coefficient but decreased the CHF. Following this study, Chen et al. (2002) concluded that a dilute spray with large droplet velocities was more effective in increasing CHF than a denser spray with lower velocities, for the same mean droplet flux. In a later paper, Chen et al. (2004) investigated spray cooling efficiency and concluded that the efficiency was affected by the mean droplet flux, Sauter mean diameter, and droplet velocity, when two of the three were kept constant. In addition, they found that CHF varied with mean droplet flux and droplet velocity, and was independent of the Sauter mean diameter, concluding that in order to achieve maximum CHF with minimum water use, one needs to select nozzles producing small diameter droplets and large droplet velocities.

Ghodbane and Holman (1991) carried out experiments using full cone circular and square nozzles with three differ-

ent nozzle diameters and sub-cooled Freon-113. They varied the flow rates, spray droplet velocity, droplet diameter, and the distance between nozzle and the heat source for cooling heat fluxes. The results of their experiments indicated that heat transfer characteristics were independent of the heat source surface area, as long as the spray was uniform, heat transfer increased with the coolant's mass flux, and that the Weber number played a significant role in the heat transfer.

Oliphant et al. (1998) compared liquid jet array cooling to spray impingement cooling in the non-boiling regime. They found that spray cooling could provide the same heat transfer coefficient as jets at a significantly lower mass flux of the working fluid, attributing the effectiveness of the spray cooling to the unsteady boundary layer created by the drops landing on the surface and the evaporative cooling provided by the drops.

Shiina et al. (2000) experimentally investigated an impinging jet, comparing it to a double nozzle spray and to an array of spray nozzles in order to compare the performance of all three in cooling a cylindrical roller. They concluded that for the single spray nozzle, the average heat transfer showed dependence on the flow rate of the water used to create the spray but not on the distance between the nozzle and the heated surface for the distances they considered. For two or more nozzles, they noted that the flow rate was still the dominant factor in cooling performance, with the geometric arrangement of the nozzles having some effect. Fabbri et al. (2003) also conducted a comparative study of spray and multiple-jet cooling, gearing it toward high heat flux applications. The jets employed were micro-jets with jet diameters of 50–150 μm. They found that small diameter micro-jets had better heat removal capacities than large micro-jets, with liquid mass flow rates similar to those of sprays. Spray cooling outperformed the micro-jets in heat removal, except for a few cases at higher flow rates, where the micro-jets performed equally well.

Although a lot of work has been carried out on sprays and spray cooling, there have been a very limited number of investigations that implemented active control of sprays to improve their cooling efficiency, where active flow control is defined as affect the behavior of a flow such that it is different from its natural state (Gad-el-Hak, 2000). Bachalo et al. (1993) noted that there are interactions between droplets of a spray and coherent flow structures. Wang et al. (1999) used a piezo-electric actuator upstream of the nozzle to modulate the spray and affect spray characteristics, concluding that it was a viable method to alter spray cone angle, droplet size, and velocity, as well as spray structure. Miller et al. (2000) used a system of four Coanda jet actuators in the outer swirl cup of a fuel injector and found that these actuators could be used to significantly increase the spreading rate of the spray. Sujith et al. (1997) investigated the behavior of droplets in axial acoustic fields, finding that the size and mean terminal velocity of the droplets were reduced in the acoustic fields. In later works Sujith (2003, 2005) showed that imposing axial acoustic fields on air atomized ethanol sprays shortened the spray, increased the spray cone angle, and reduced the droplet velocity, which the author attributed to the presence of smaller droplets.

Active flow control has also been used in combustion applications (e.g., Dubey et al., 1997; Zhu et al., 2002; Ramanaryanan et al., 2003; Benajes et al., 2005) and in agriculture in the presence of a cross-flow (e.g., Giles et al., 1995; Ghosh and Hunt, 1998; Farooq et al., 2001). The studies in combustion showed that active flow control is a viable method to affect the development of the spray as well as the droplets themselves (e.g., their size), while the studies of the interaction of sprays with cross-flow are useful for active flow control design implementation. The effect of cross-stream on the spray development resembles the case in the present work, when a single synthetic jet is activated, as discussed below.

There is only one published work, known to the authors, which addressed the possibility of using active flow control on sprays in order to enhance heat transfer. Namely, the study by Panao and Moreira (2005) who investigated spray impingement of pulsed sprays on heated surfaces for conditions that are representative of IC engines. They found that manipulating the nature of droplet impingement on the heated surface, accomplished by pulsating the sprays, can enhance heat transfer. Therefore, the motivation of the present work is to explore the feasibility of using synthetic-jet-based active flow control to affect the spray characteristics, which can then be implemented in spray cooling of a heated surface in the non-boiling regime.

2. Experimental setup and procedure

Active control of sprays was investigated using synthetic jets and was applied in spray cooling of a hot surface in the non-boiling regime. Therefore, a special facility was designed (Fig. 1), consisting of an enclosure that allowed non-intrusive optical measurement techniques and accommodated a spray nozzle, equipped with a flow control module, as well as an insulated heater for spray cooling measurements. The enclosure featured a 485 mm × 425 mm × 435 mm volume with an open top and a drain in the bottom. The spray nozzle, instrumented with a flow control module, was mounted above the enclosure, attached to a micrometer slide with the resolution of 0.06 mm for position control of the spray orifice location in the vertical direction. The position of the spray nozzle above the enclosure allowed for optical measurements of the spray parameters while minimizing ricocheting of droplets off the walls and bottom, which could obscure the measurements. For the heat transfer experiments, the heater module was stationed beneath the spray at the bottom of the enclosure.

In the present experiments, water was used as the working liquid, and the spray was created using an air-assisted atomizing nozzle from Delavan (model 30609-2), featuring

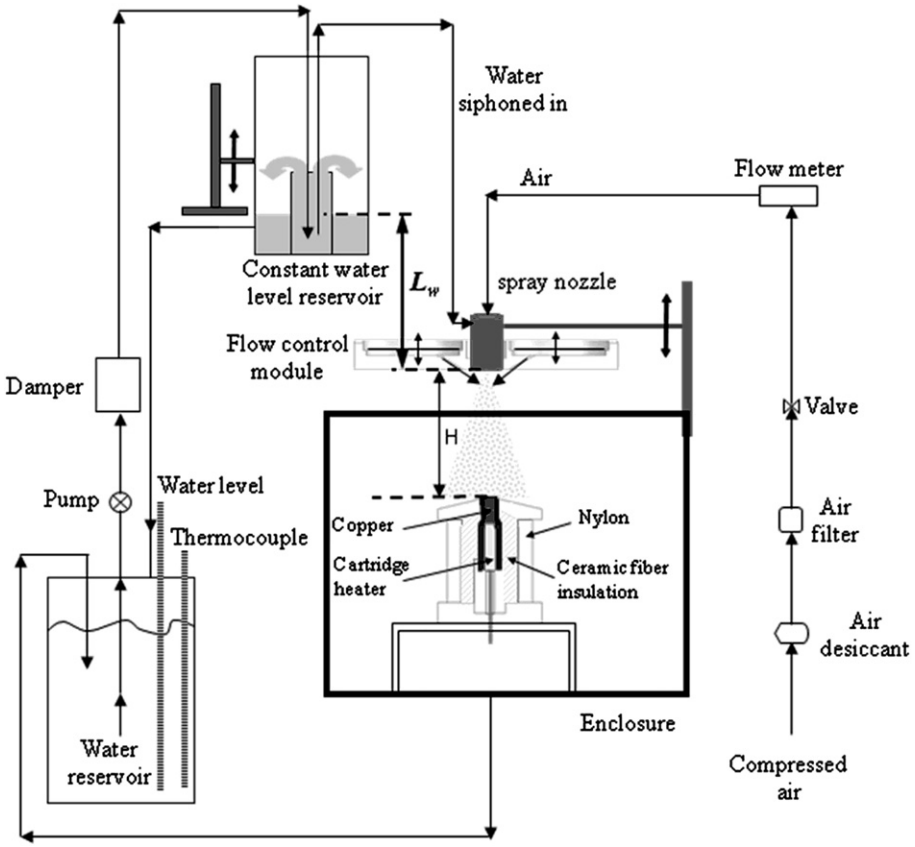

Fig. 1. Experimental setup of the spray cooling.

an orifice diameter of 1.7 mm. A constant water level reservoir was used to accommodate the spray nozzle. It was comprised of a small open top container, positioned within a larger open top container with a return drain. The smaller container received a continuous supply of water that was allowed to overflow into the larger container, thereby creating a reservoir that was always filled to the same level (point of overflow) from which water was siphoned. The larger container was mounted on a motorized, computer controlled traverse, allowing the water intake to be at a range of L_w of 0–490 mm above the level of the spray nozzle orifice. Thus, a precise control of the amount of water siphoned, for a given air flow rate, was enabled. Note that the water flow rate through the spray nozzle depended on two parameters: the water intake level elevation L_w, and the air flow rate (the relationship between the water flow rate and the air flow rate was presented in our previous papers, Pavlova et al., 2007, 2008). Water was pumped from a 37.9 l container, equipped with a water level meter and a type-T thermocouple, by a diaphragm pump through a closed 7.6 l pressure vessel, which was used to damp out the unsteadiness associated with the pump.

Air flow to the nozzle was provided with a pressurized air line that passed through a dryer to remove the moisture and a filter to eliminate any particles larger than 5 μm, followed by a regulating valve and an in-line flow meter (Sierra 826). The air flow rate was monitored by a LabVIEW program, which averaged 1000 flow rate measurements per second and allowed volumetric flow measurements to within 3%, such that the flow rate of the air supplied to the nozzle could be set and regulated by adjusting the valve throughout experiments. In the present experiments, the air flow rate was varied from 5.5 l/min to 16.5 l/min. Water mass flow rates were measured for the three values of water intake elevation with respect to the nozzle face, L_w, used in the present experiments (0, 245, and 490 mm, respectively) at five air flow rates, Q_a. Volumetric flow rates for the water, Q_w, were then calculated based on the mass flow rates. The maximum uncertainty associated with these measurements was estimated to be less than 5%.

The flow control module fitted onto the spray nozzle, such that the spray nozzle was in the center, and four synthetic jet actuators, located around the circumference of the spray nozzle, are at 90°; to each other (Fig. 2). Each synthetic jet was driven with a 31.2 mm diameter and 1.3 mm thickness piezo-electric disk (operating in mode I oscillations) that through a 5 mm in length and 0.5 mm in width slit orifice at 7.3 mm from the spray orifice center. The synthetic jets were inclined 30° with respect to the plane of the nozzle orifice to allow vectoring of the spray (when a single jet was used) or focusing of the spray (when all four jets were activated simultaneously). The inclination angle of the synthetic jet was selected such that the jet

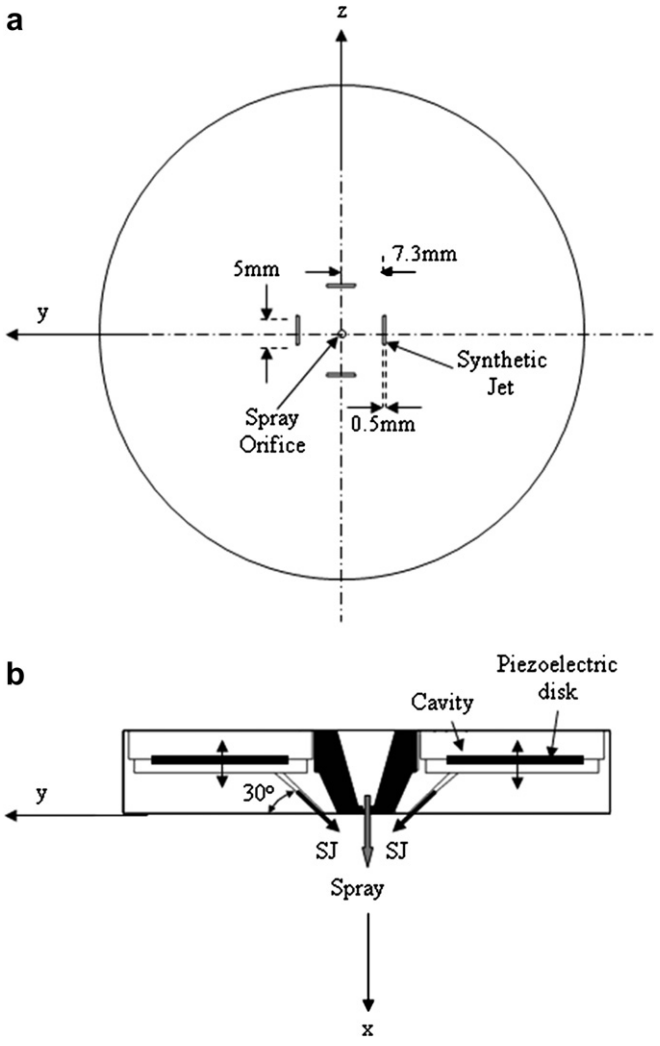

Fig. 2. Flow control module instrumented with synthetic jets.

impacted on the spray downstream of the developing region of the spray.

A synthetic jet is a jet that is formed at the edge of an orifice due to the periodic motion of a diaphragm, mounted on one of the walls of a sealed cavity. The synthetic jet is zero-net-mass flux in nature but it allows momentum transfer to the flow. With a proper design, the system is driven near resonance; thus, small electrical power is needed. Furthermore, no mechanical complexities or plumbing are needed, which makes them attractive for flow control applications. For more details about synthetic jets see the review by Glezer and Amitay (2002).

The strength of the synthetic jets was quantified using the momentum coefficient, which is the ratio of the synthetic jet momentum to the spray momentum, defined as

$$C_\mu = \frac{nA_j U_o^2}{A_s U_e^2}, \tag{1}$$

where n is the number of synthetic jets used, A_j is the area of the synthetic jet orifice, A_s is the area of the spray orifice, U_e is the average air exit velocity at the spray orifice (based on the measured air flow rate), and U_o is the synthetic jet average orifice velocity (based on the work by Smith and Glezer, 1998), defined as

$$U_o = \frac{L_o}{\tau}, \tag{2}$$

where L_o is the synthetic jet stroke length, defined as

$$L_o = \int_0^{\tau/2} u(t)\,dt, \tag{3}$$

where $\tau = 1/f$ is the cycle period, f is the driving (formation) frequency of the jet, and $u(t)$ is the periodic centerline velocity at the jet exit plane. In the present experiments, the synthetic jets were driven with a sinusoidal waveform at a frequency of 1100 Hz. This frequency was selected such that it corresponds to the optimal driving frequency (i.e., strongest jet with a minimum input power) for the system of the piezo disk and the cavity used. Note that the synthetic jets in the module were calibrated using hotwire anemometry prior to spray experiments (similar to the work by Smith and Glezer, 1998). As was shown by multiple researchers (e.g., Pothos, 2002; Pothos and Longmire, 2002), particle/droplets-laden flows are affected by either a direct mechanism (direct momentum transfer to the particles/droplets) or indirectly (due to the amplification of coherent structures in the carrier fluid that indirectly affect the particles/droplets). Since the Strouhal number (based on the spray diameter, the average carrier air velocity at the orifice and the driving frequency) varies from 0.016 to 0.047 for the range of air flow rates used, it is an order of magnitude lower than the unsteady modes of the flow. Therefore, the frequency here is used only to form the jet and not to excite the coherent structures in the carrier air flow of the spray. Hence, the flow control here is a direct mechanism only.

Global spray measurements were carried out with Particle Image Velocimetry (PIV), which provided velocity fields for the spray droplets for an interrogation window of 65.5 mm by 49.5 mm (with a spatial resolution of 0.38 mm). The PIV data were acquired for five air flow rates, three water intake level to nozzle level distances, L_w, and for three momentum coefficient values, C_μ, at each setting. The PIV system is based on the commercially available LaVision hardware and software and utilizes two 120 mJ Nd:YAG lasers and a 1376×1040 pixel resolution thermo-electrically cooled 12-bit CCD camera. The laser sheet was aligned with the center of the spray, and the CCD camera was mounted perpendicular to the laser light sheet. For each case, a set of 2000 double images was recorded, and averaged velocity fields were computed. In these measurements, no flow tracers were added to the air flow; therefore, the velocities that were measured in this two-phase flow were the velocities of the water droplets themselves, but not of the air present in the spray, as the water droplets are too large and heavy to faithfully follow the air motion (the average Stokes number of the droplets along the centerline is in the order of 20). All velocity

vectors were calculated using a cross-correlation technique with adaptive multi-pass, deformable interrogation windows (single pass at 32 × 32 and two passes at 16 × 16 pixels) with 50% overlap. The camera was mounted at a perpendicular distance of ~0.35 m to the laser light sheet such that the distance between pixels was 47.6 μm. Maximum velocity (~23 m/s) in these experiments corresponded to an average displacement of approximately 5.3 pixels with an error of approximately ±0.1 pixel (corresponding to velocity error of ±0.4 m/s).

A heater module was designed and fabricated for spray cooling experiments and stationed below the spray nozzle for spray cooling experiments. The module consisted of a 400 W maximum output cartridge heater by Omega, embedded in an oxygen-free piece of copper, the top surface of which was a flat circle with a diameter of 19 mm that was exposed to the spray. The copper piece had 15T-type thermocouples from Omega, 0.2 mm in diameter each, embedded in the cylindrical top region with thermally conductive epoxy (with a thermal conductivity of 1.04 W/m K compared to 400 W/m K of the copper) used for attachment. The locations of thermocouples within the heater top are illustrated in Fig. 3. Before the thermocouples were placed inside the copper, they were calibrated with respect to each other, as well as to the thermocouples that measured the room temperature and the water temperature. The top array of thermocouples was 2 mm below the surface; an identical array was placed 2 mm below it, and there was also a central thermocouple 2 mm below the second row in the center, so that heat flux through the top of the heater could be calculated. Attaching thermocouples directly onto the surface was impractical in this application, and could lead to serious measurement errors (Tszeng and Saraf, 2003); therefore, temperature values at the surface were obtained from extrapolation. The thermocouples were located in two rows, along the y-axis and the z-axis and are 3.2 mm from each other. This arrangement of thermocouples allowed for a spatially resolved set of temperature measurements in the heated surface as well as heat flux calculations.

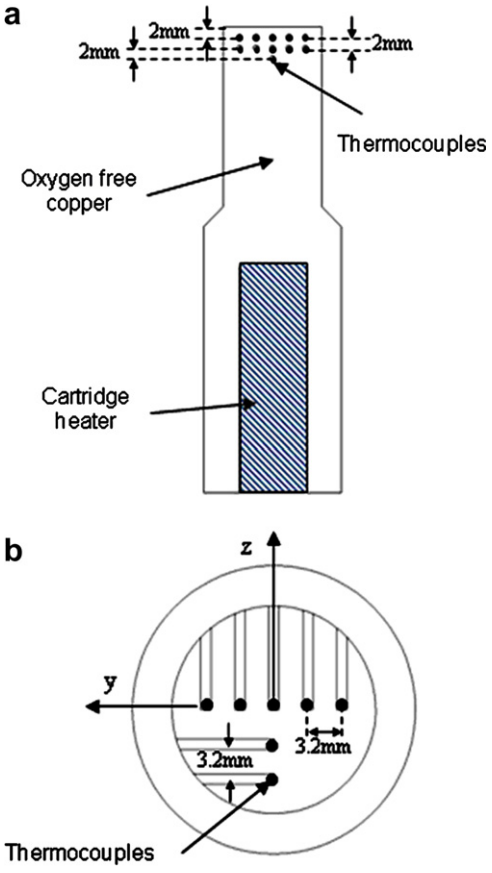

Fig. 3. Copper heater with thermocouple locations.

In order to minimize heat losses from the copper piece, it was placed inside an insulation sleeve, which was comprised of a solid nylon cylinder on the outside and ceramic fiber insulation by DuraBlanket (thermal conductivity, $k = 0.01$ W/m K) immediately surrounding the copper. The outer diameter of the insulation sleeve was 105 mm. The neck region of the heater, leading up to the exposed surface, was also surrounded by the ceramic fiber insulation, and a slanted nylon cap was placed on top, to allow the liquid to drain off the sides.

Based on the temperature calibrations and error associated with extrapolation of temperatures up to the surface, the maximum uncertainty of ΔT was calculated to be about 2%. The uncertainty of heat flux out of the exposed heater surface was associated with the error in the measured ΔT and the location of the thermocouples in the vertical direction, and was estimated to be less than 6.5%, based on tolerances specified in making the copper portion of the heater. Assuming that errors are independent, it was reasonable to estimate the overall uncertainty heat flux through the top of the heater calculations, based on the method of Kline and McClintock (1953), which resulted in calculated heat flux uncertainty of less than 8.5% for all heat transfer experiments presented in this paper. The uncertainties in the air to water flow rate ratio, Q_a/Q_w, based on the error associated with the flow meter and the error estimated for the water flow rate measurements was at most 10%. The uncertainty of velocity, based on the specifications of the PIV system used and as described above, are within 3%.

Detailed spray characteristics (droplet size, concentration, and distribution of individual droplets) were obtained using the Shadowgraphy technique. This technique is based on high resolution imaging and backlight illumination, where solids, opaque or transparent droplets, and bubbles having a diameter from 2 μm to 2000 μm can be measured. A laser beam passes through a diffuser, such that the droplets are illuminated from one side, and a high resolution CCD camera (instrumented with a long-range microscope) acquires images of the shadows from the opposite side. The same dual-pulse laser was used as for the PIV experiments, along with a special diffuser attachment for scattering the laser light. The CCD camera with a long-range microscope

attached, and the light source were mounted on an optical table. Shadowgraphy measurements were acquired at 45 locations in the spray, such that the effect of active flow control could be determined for the entire three-dimensional spray. In the present paper, only data along the centerline of the spray are presented for brevity [for more details about the Shadowgraphy technique, including a complete description of droplet sizing and velocity measurements, as well as for the full 3D field, see previous work by Pavlova et al. (2007, 2008)]. In these measurements, the resulting uncertainty in the velocity is ±0.1 m/s and ±0.5 μm in the droplet diameter.

3. Results

3.1. Flow control of sprays

The effect of a single synthetic jet on the global characteristics of the spray was explored when the synthetic jet was driven with a range of momentum coefficients from 0.005 to 0.425 (with a corresponding velocity ratio, U_o/U_e, range of 0.5–1.5). The spray parameters include a range of air to water volume flow rate ratios, Q_a/Q_w, from 166 to 746, for which L_w/d_s was varied between 0 and 288. For brevity, data for spray with $Q_a/Q_w = 166$ (and $L_w/d_s = 288$) are presented here; however, similar results were obtained for other flow rate ratios.

Fig. 4a–d presents the velocity vector field of the spray, where Fig. 4a presents the baseline (no flow control) case, and Fig. 4b–d shows the cases with flow control, having $C_\mu = 0.04$, 0.20, and 0.425, respectively (the orientation of the measurement plane is shown in the inset). Without flow control the spray is symmetric with a spreading angle of ~27°, where the edge of the spray is defined as the location where the streamwise velocity is 20% of the maximum velocity of the spray. The 20% cutoff was used due to the fact that some droplets hit the bottom of the enclosure and bounce back and thus contaminate the velocity field. This is more pronounced near the edges of the spray, where the droplets' velocity is smaller. For velocities larger that 20% of the maximum velocity the droplets can be considered a part of the spray with confidence. This is consistent with the spray angle value of 30°, provided by the manufacturer.

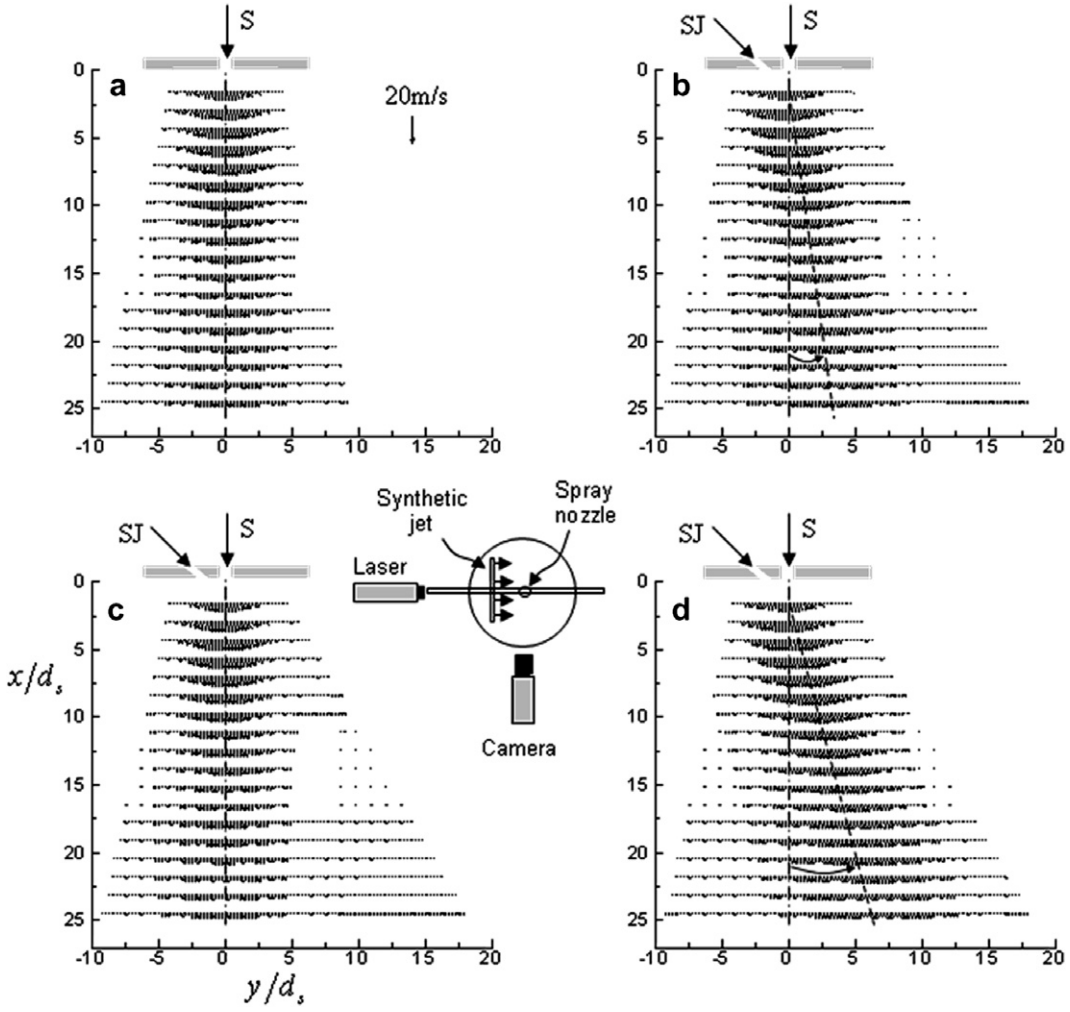

Fig. 4. Velocity vectors fields of the baseline (a) and forced spray with $C_\mu = 0.04$ (b), 0.20 (c), and 0.425 (d). $Q_a/Q_w = 166$, and $L_w/d_s = 288$.

When the synthetic jet is activated with the smallest C_μ (Fig. 4b) the effect is miniscule. As C_μ increases, the spray is vectored away from synthetic jet with a vectoring angle of $\theta = 9°$; and 18°; for $C_\mu = 0.20$ and 0.425, respectively. The vectoring angle is defined as the angle between the x-direction and the line that follows the maximum spray velocity. Another measure of the spray modification by the synthetic jet is the effect on the downstream evolution of the centerline velocity, and the spreading rate of the spray. Without flow control, the normalized centerline velocity increases very rapidly for approximately $x/d_s < 6$, where the maximum occurs. Farther downstream, the centerline velocity decays with downstream distance as $(x/d_s)^{-0.5}$, which is consistent with the findings of Faeth et al. (1995) and Cossali (2001). When the synthetic jet is activated, there is a small effect near the orifice, while the spreading of the spray is significantly enhanced farther downstream. For detailed information on the behavior of the spray when a single synthetic jet is used for flow control, as described above, refer to (Pavlova et al., 2008).

Another important spray parameter that can have a significant contribution to the spray's ability to remove heat is its velocity RMS level. Therefore, the effect of the synthetic jet on the normalized streamwise and cross-stream RMS velocity components were measured, and are presented in Figs. 5a–b and c–d, respectively, for $Q_a/Q_w = 166$ and $C_\mu = 0.425$. As expected, without control, the RMS fields of each velocity components is symmetric with respect to the centerline, and it exhibits a double peak distribution (one peak on each side of centerline) for $2 < x/d_s < 7$. Farther downstream, the cross-stream distributions of both RMS components have a single peak, where the maximum levels are around the centerline. Note that the RMS magnitudes, throughout the flow field, of the cross-stream velocity are larger than the values of the streamwise component. When the synthetic jet is activated the RMS levels increase throughout the flow field and the distribution is not symmetric.

Previous work (Camci and Herr, 2002) showed that imposing a flapping motion on an impinging jet cooling resulted in an increased heat transfer from the surface. Therefore, the effect of flapping on spray cooling was investigated (presented in Section 3.2). In order to achieve this type of motion, two opposing synthetic jets were used, and were driven with a ramped function in order to achieve gradual sweeping of the spray from one side to another (see the schematic in the bottom of Fig. 6).

Fig. 6 presents the velocity vector field of the spray for the flapping experiments, where the full sweeping cycle, τ_p, takes course over 1 s (the effect of the duration of the cycle on the heat transfer, for cycle times from 0.5 to 2 s, was similar and thus not presented). The flapping time was selected to be about an order of magnitude larger than the droplet's residence time (e.g., corresponding to the time

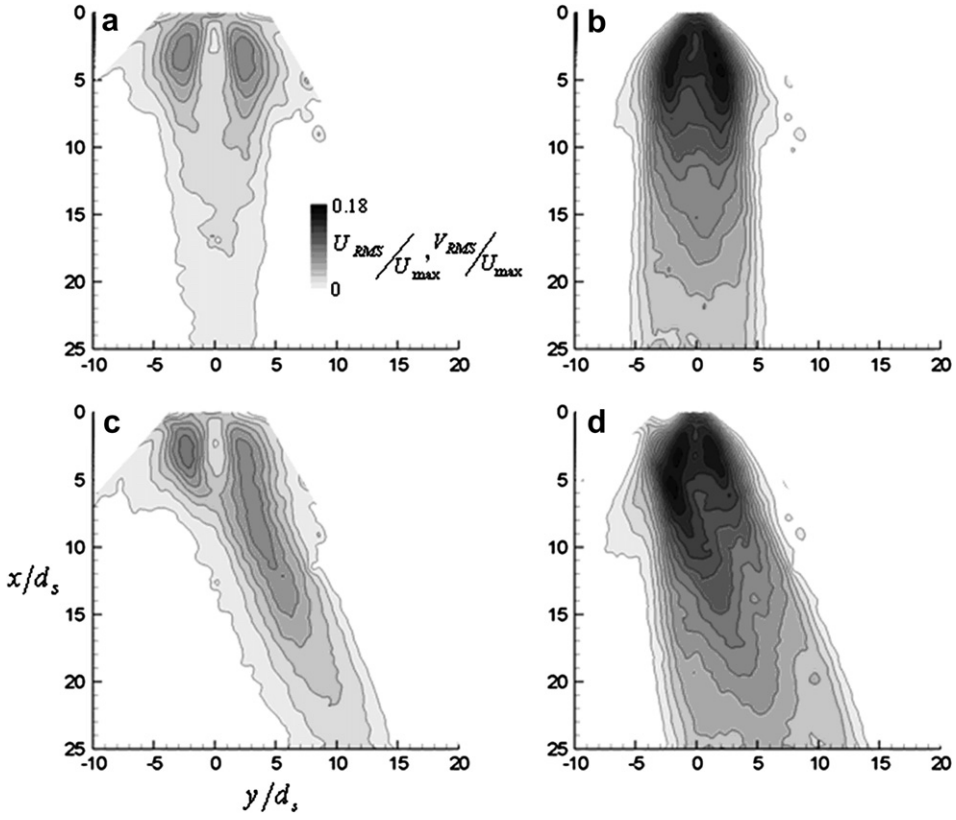

Fig. 5. The streamwise and cross-stream components of the velocity RMS fields for the baseline (a, c) and actuated with $C_\mu = 0.425$ (b, d) sprays. $Q_a/Q_w = 166$ and $L_w/d_s = 288$.

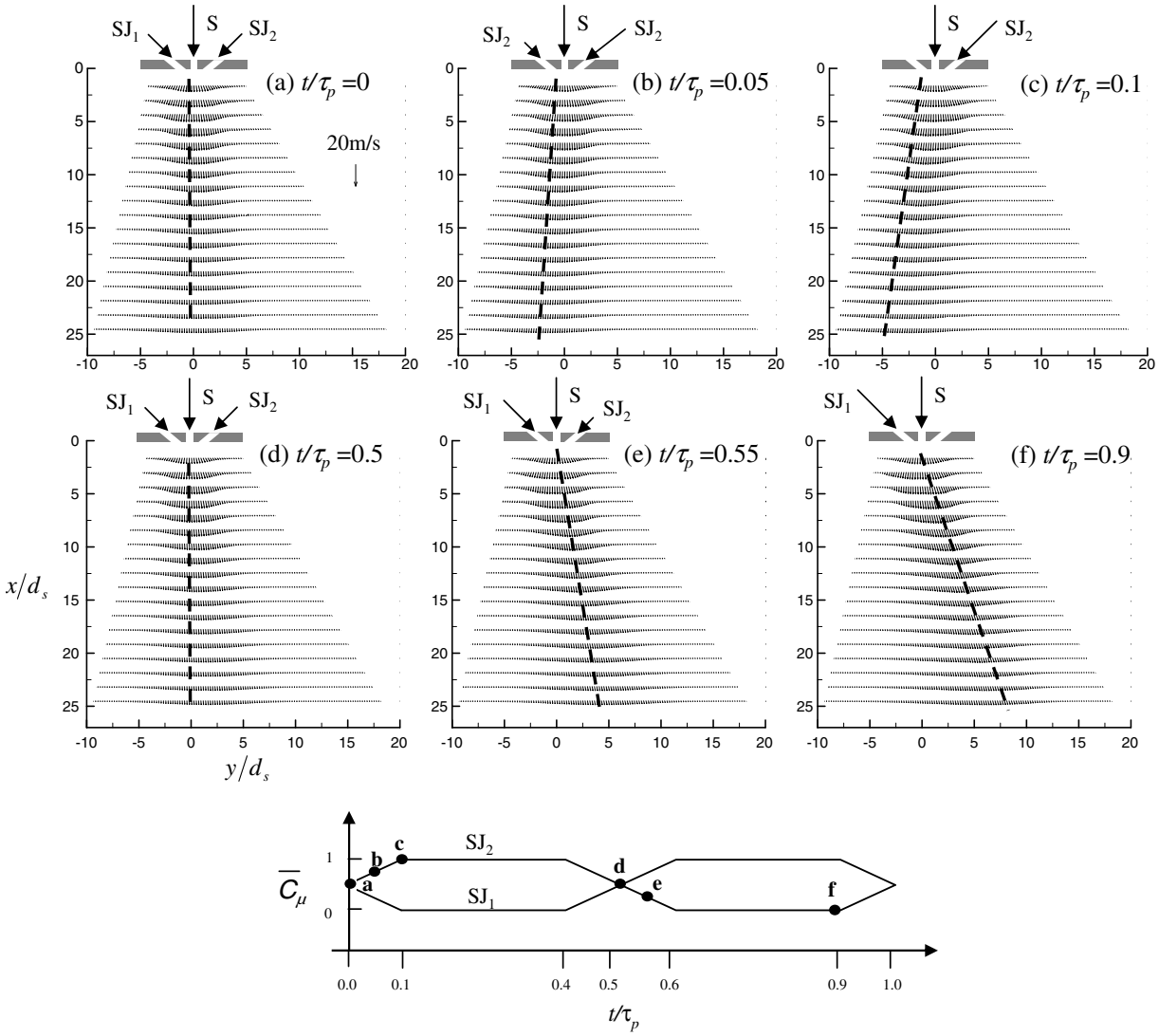

Fig. 6. Velocity vector fields at different times during the flapping motion. $Q_a/Q_w = 166$ and $L_w/d_s = 288$.

it takes the droplets to reach the surface and to travel along the hot surface) to ensure complete removal of the droplets/liquid from the hot surface. In each vector field, the relative strength of the synthetic jets on the left (SJ_1) and right (SJ_2) of the spray is represented by the length of the arrows.

At $t/\tau_p = 0$ (Fig. 6a) both synthetic jets have the same strength; thus, resulting in a symmetric (about the x-axis) spray with no vectoring to either side. At $t/\tau_p = 0.05$ (Fig. 6b), the right synthetic jet (SJ_2) is stronger than the left jet (SJ_1), as the amplitude of the right synthetic jet is ramped up while the amplitude of the left synthetic jet is ramped down, and the spray is vectored to the left with an angle of ~4°. As time progresses to $t/\tau_p = 0.1$ (Fig. 6c), the left synthetic jet is off, and the right synthetic jet is at its maximum strength, resulting in further vectoring of the spray to the left with an angle of ~10°. At mid-cycle, the spray is returned to its original position, as the left synthetic jet is ramped up while the right synthetic jet is ramped down, resulting in control jets of equal strength (Fig. 6d), and thus a symmetric spray. At $t/\tau_p = 0.55$ (Fig. 6e), the left synthetic jet is stronger than the right, resulting in a spray that is vectored to the right with an angle of ~7°. Finally, as the left jet is at its maximum strength and the right jet is off, the spray is further vectored to the right with the angle of ~12° (Fig. 6f). The slight difference in the spray angle that occurs in this sweeping motion is due to the fact that the synthetic jets might not have been perfectly matched in strength.

In addition to the gradual flapping motion, on–off flapping was also implemented when the two opposing jets were driven with a step function, such that when SJ_1 is on, SJ_2 is off, and vice versa. The resulting spray velocity vector fields are similar to those presented in Fig. 6c and f. Both flapping methods were used to improve the efficiency of the spray cooling, and are presented in Section 3.2 below.

As was discussed in the introduction, the size of the droplets, their concentration, and distribution have

significant effect of the cooling efficiency. Therefore, the effect of the synthetic jet on these parameters was also investigated. Data were acquired in three x–y planes, where 15 data points were measured at each plane, as shown schematically in Fig. 7. For brevity, data are presented only for the centerline plane (detailed results are presented in recent work by Pavlova et al. (2007, 2008).

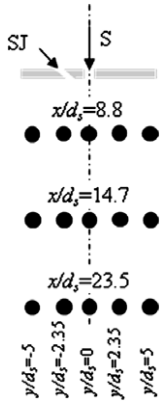

Fig. 7. Locations for the detailed measurements.

Fig. 8a–c presents the droplet size distribution histograms for the baseline spray, $N_{d_b}/N_{d_b}|_{\text{total}}$, while Fig. 8d–f shows the percentage change (with respect to the baseline case) in the droplet diameter, $\%\ (N_{d_f-N_{d_b}})/N_{d_b}$, for the controlled cases at three x/d_s locations. Here, $N_{d_b}/N_{d_b}|_{\text{total}}$ is the number of droplets at a given size range, normalized by the total number of droplets throughout the interrogation window, and N_{d_b} and N_{d_f} are the number of droplets (for a given group size) in the interrogation window for the baseline and forced case, respectively. For each droplet size group, five cross-stream locations are presented, indicated by the different styles of bars.

The histograms of the baseline spray exhibit a high concentration of droplets having a diameter between 8 μm and 12 μm, where ~85% of the droplets have a size between 4 μm and 20 μm at all three downstream locations (Fig. 8a–c). At $y/d_s = \pm 2.35$, for all three downstream locations, the most prevalent droplet size is still between 8 μm and 12 μm; however, there are more droplets of larger

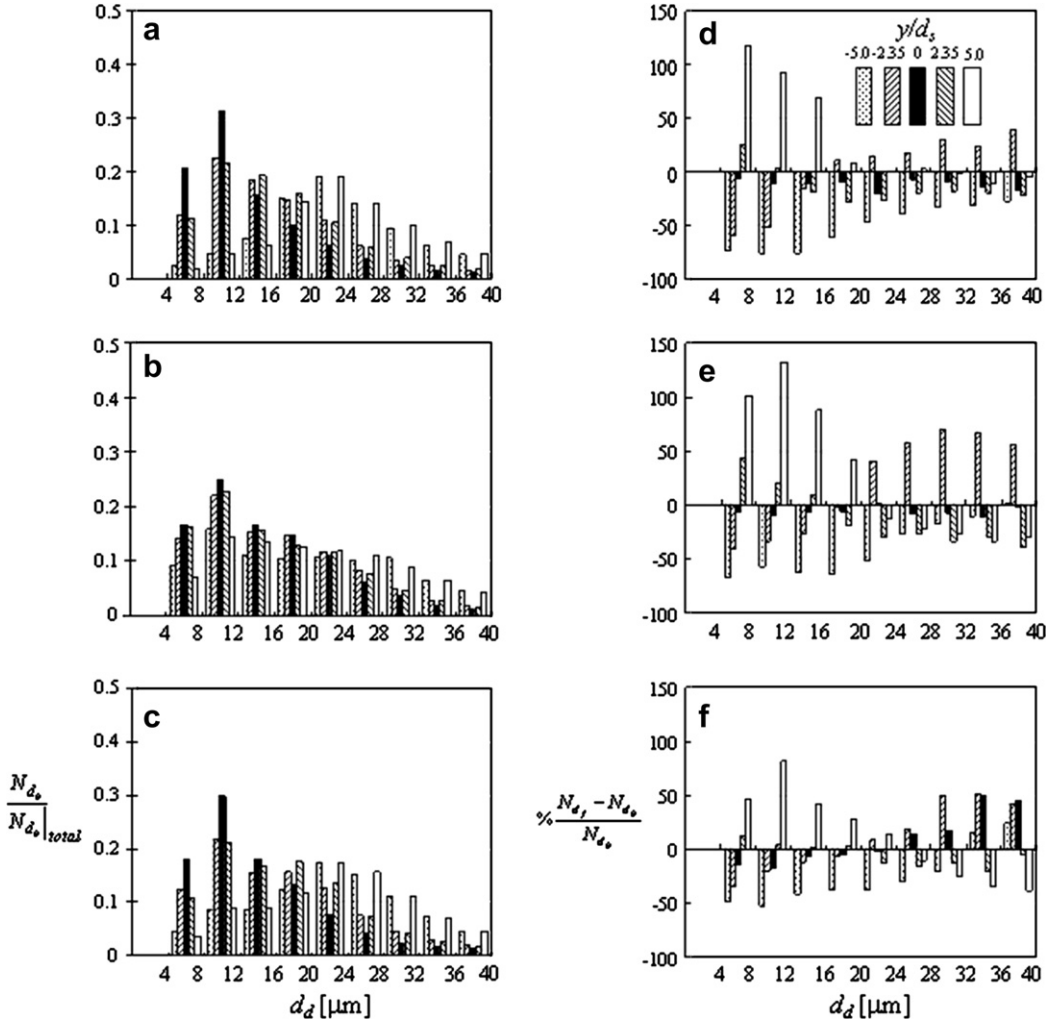

Fig. 8. Droplet size distribution histograms for the baseline spray, $N_{d_b}/N_{d_b}|_{\text{total}}$ (a–c), and the percentage change (with respect to the baseline case) in the droplet diameter, $\%\ (N_{d_f} - N_{d_b})/N_{d_b}$ (d–f).

diameters than at the centerline. Farther off the centerline (at $y/d_s = \pm 5$), there is a high concentration of droplets with a diameter between 20 μm and 24 μm. Note the symmetric distribution of droplets about the spray centerline.

When the synthetic jet is activated (Fig. 8d–f) there is a decrease in the number of small droplets on the left side of the spray (i.e., the side closer to the synthetic jet) and an increase of those same small droplets on the right side of the spray, indicating that small droplets ($4\ \mu m \leqslant d_d \leqslant 16\ \mu m$) are pushed to the right side of the spray (i.e., away from the synthetic jet) due to the impulse of the synthetic jet on the droplets. Also, there are more droplets of large

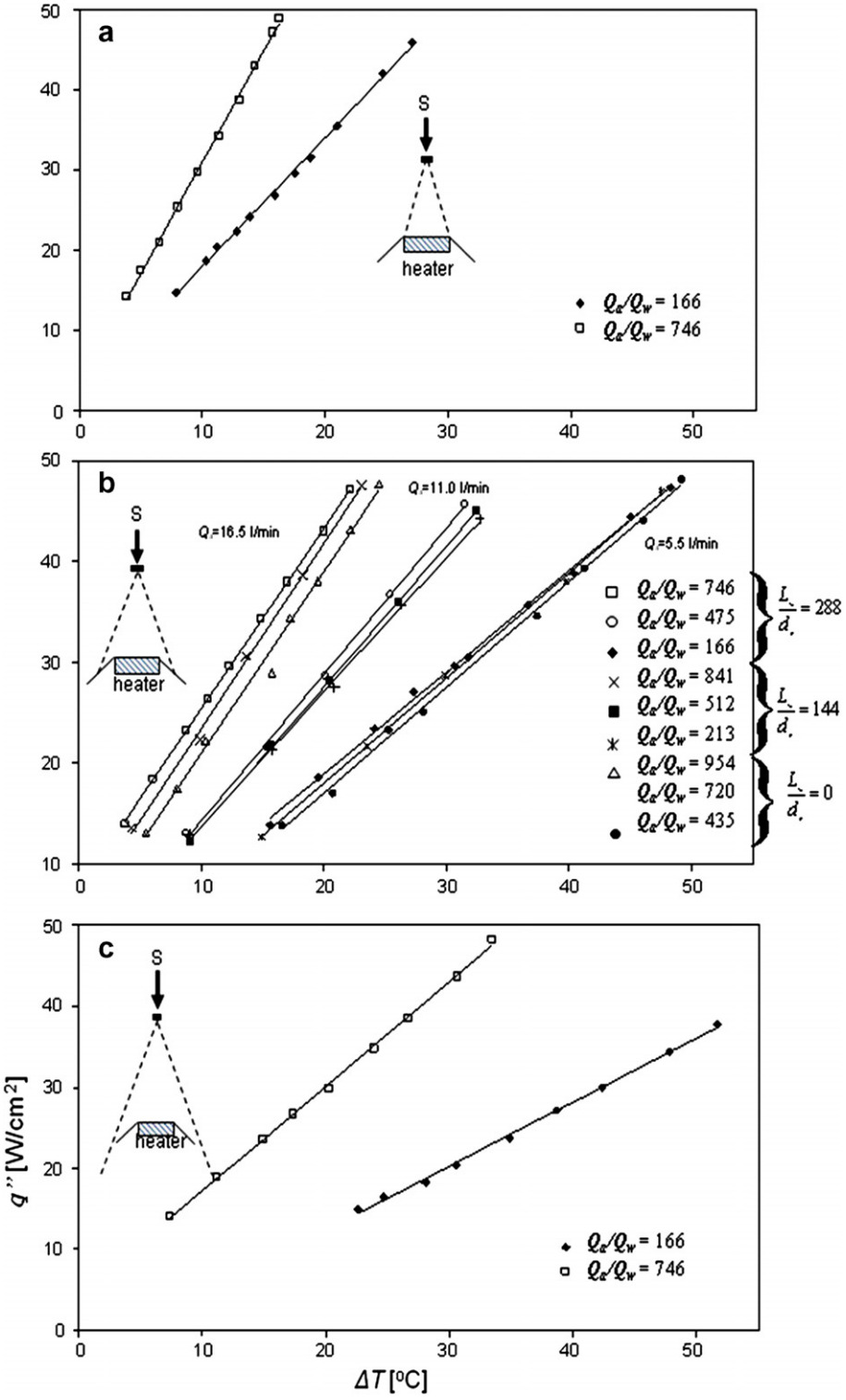

Fig. 9. Heat flux through the top of the heater *vs.* ΔT at $H/d_s = 23.5$ (a), $H/d_s = 35.3$ (b), and $H/d_s = 47$ (c). Baseline spray.

diameters to the left of the spray centerline and fewer to the right side, compared to spray without flow control. A plausible explanation for this is that as the small droplets are pushed towards the spray centerline, some of them coalesce with other droplets on the left side of the spray, creating larger droplets.

3.2. Active control of spray cooling

Next, the effect of the synthetic jets on the spray cooling efficiency was explored. First, baseline cases of spray cooling (i.e., without flow control) were acquired for three distances between the heater and the spray nozzle, H/d_s, and

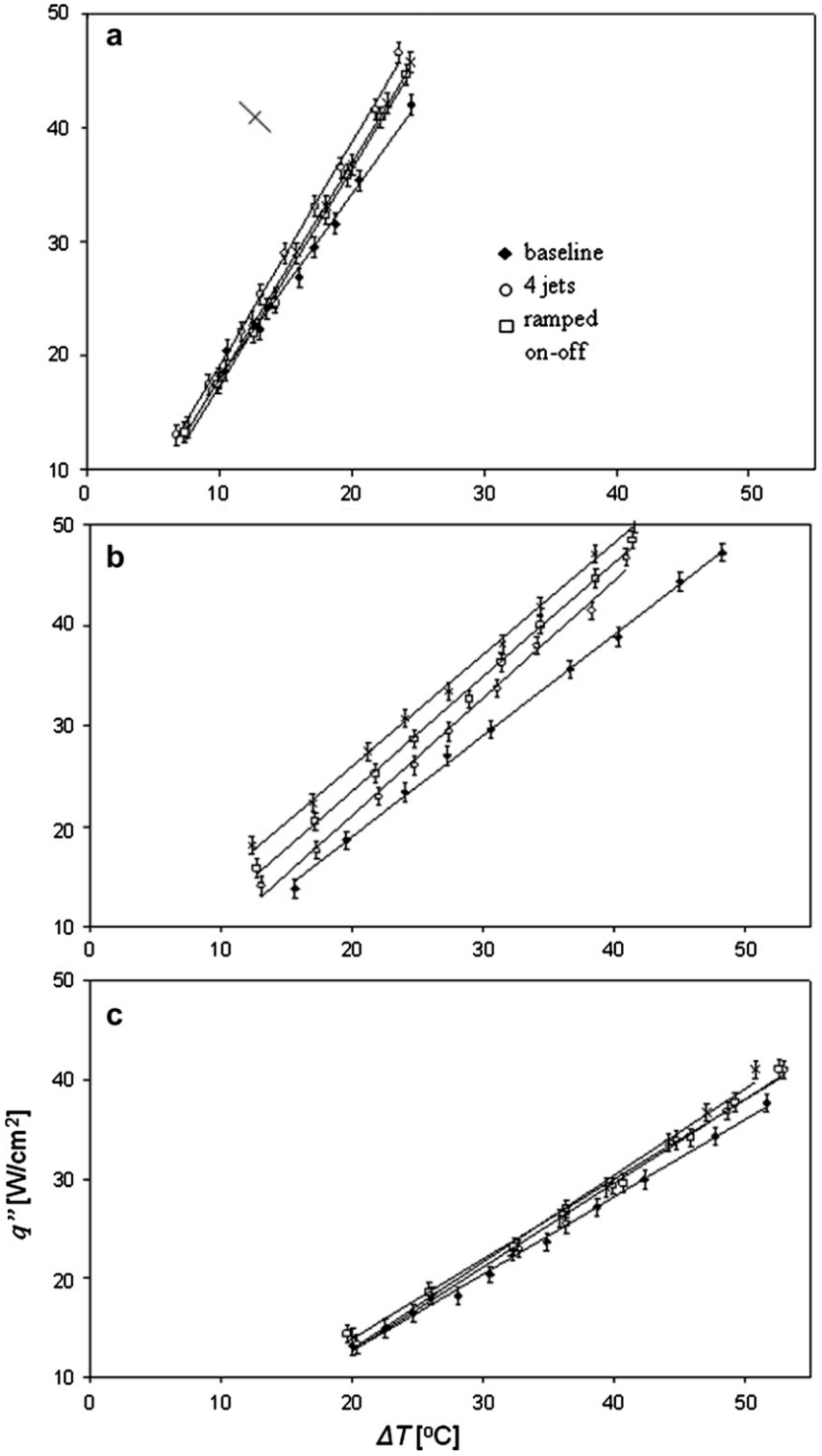

Fig. 10. Heat flux through the top of the heater *vs.* ΔT at $H/d_s = 23.5$ (a), $H/d_s = 35.3$ (b), and $H/d_s = 47$ (c). Controlled spray.

different Q_a/Q_w. Temperature data were recorded at several heat flux settings for each case, and the heat flux values were calculated.

Fig. 9 presents the heat flux removed from the surface *vs.* ΔT (temperature difference between the heater surface and the water, with water being at room temperature) at $H/d_s = 23.5$, 35.3 and 47 (Fig. 9a, b and c, respectively). Note that each plot shows a schematic illustrating the relative coverage area of the spray at the specific H/d_s with respect to the area of the heater. For all cases the relationship between the heat flux and ΔT is linear (R^2 is 0.99 or better), as also noted by other researchers (Jia and Qiu, 2003; Kim et al, 2004; Hsieh and Yao, 2006).

At $H/d_s = 23.5$ (the shortest distance between the heated surface and the spray nozzle used in the present experiments, Fig. 9a) spray cooling results in the highest heat removal at a given ΔT (compared to larger surface to spray distances, Fig. 9b and c). Moreover, for the same heat flux (based on the average of seven thermocouples), ΔT is decreased by as much as 45%, for the higher flow rate ratio case, compared to the lower flow rate ratio case.

At $H/d_s = 35.3$ (Fig. 9b), data at nine flow rate ratios were collected, a set of three air flow rates (5.5 l/min, 11 l/min, and 16.5 l/min) at three normalized distances between the water intake level and the face of the spray nozzle, $L_w/d_s = 0$, 144, and 288. Note that for a given air flow rate, as L_w/d_s increases Q_a/Q_w decreases, as the volumetric flow rate of water increases when the nozzle siphons from a higher location (see Pavlova et al., 2007, 2008).

Fig. 9b shows that for each set of L_w/d_s, the relationship between the heat flux and ΔT is linear, where the data were acquired at the same air flow rate and at the three L_w/d_s locations. At this nozzle-to-heater distance, there is a big difference between the cooling performance of high, intermediate, and low air flow rates (up to 45% at high heat fluxes), as expected. The cases with the same air flow rate but an increased Q_a/Q_w (due to decreased L_w/d_s) show a slightly reduced cooling performance due to the smaller volume of water contained in the spray and lower droplets velocity.

At $H/d_s = 47$ (Fig. 9c) the effectiveness of spray cooling decreases (compared to the other two cases where the spray was closer to the hot surface). Also, as for the other two cases, the higher the flow rate ratio, the better the surface cooling. It is clear that as H/d_s increases, the heat removal from the surface decreases, which is not surprising, considering that the streamwise velocity of sprays decreases downstream of the nozzle for all Q_a/Q_w, resulting in droplets that impinge on the surface of the heater with much smaller momentum. Furthermore, as the distance between the heater and the spray nozzle increases for the same Q_a/Q_w, the cross-sectional area of the spray becomes much greater than the area of the heater, and the amount of water wasted becomes progressively larger. For example, at $H/d_s = 23.5$ the spray covers the area of the heater almost perfectly for $Q_a/Q_w = 166$, while at $H/d_s = 47$, the area of the spray covers an area that is twice the heater area.

The effect of the spray control on the heat transfer was explored by using three modes of active flow control: (1) four synthetic jets activated simultaneously, (2) ramped sweeping, and (3) on–off flapping (as discussed in conjunction with Fig. 6). It is important to note that the power required to operate the synthetic jets is very low, at most 0.4 W in the case of four jets operating simultaneously. Data were acquired for $H/d_s = 23.5$, 35.3, and 47, $Q_a/Q_w = 166$, and $L_w/d_s = 288$. All three modes of flow control had some effect on heat transfer from the surface for the three H/d_s tested, as illustrated in Fig. 10a–c. The error bars here and in Fig. 11 represent the highest estimated error, which is 8.5% of the lowest heat flux in all experiment and is the worst case scenario. At $H/d_s = 23.5$

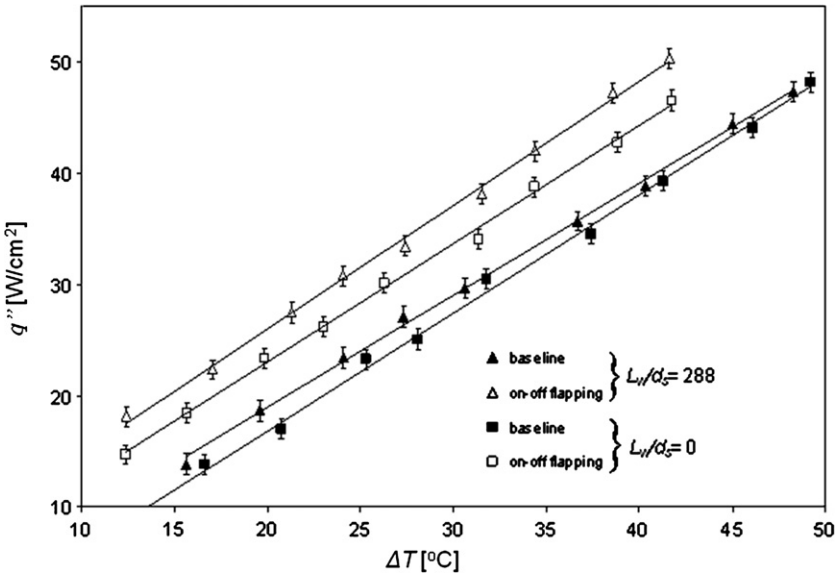

Fig. 11. Heat flux through the top of the heater *vs.* ΔT at $H/d_s = 35.3$, $Q_a = 5.5$ l/min, and $L_w/d_s = 0$ and 288.

(Fig. 10a) flow control with four jets operating together has the greatest enhancement of heat removal (for example, for heat flux of 30 W/cm^2 out of the top ΔT is 14% lower than the baseline). This is probably due to the focusing of the spray, and a higher droplets velocity (Pavlova et al., 2007).

As the distance between the spray and the hot surface was increased to $H/d_s = 35.3$ (Fig. 10b), all three modes of flow control resulted in a reduction of the surface temperature (for example, using the on–off flapping yielded a reduction in ΔT by up to 36%, compared to the baseline, at a heat flux of 18 W/cm^2 out of the top, while at 42 W/cm^2, the reduction in ΔT is 18%). The other two forms of flow control also show a cooling improvement, but to a lesser degree. At $H/d_s = 47$ (Fig. 10c), flow control resulted in a slight cooling enhancement, with all three modes of flow control producing about the same effect.

To further explore the effect of water intake elevation, L_w, on the performance of flow controlled heat removal, the three modes of flow control were compared for different L_w at the same flow rate. Fig. 11 illustrates the heat transfer enhancement by on–off flapping for sprays at the same air flow rate and at two different L_w/d_s. Both the baseline and controlled sprays at higher water intake elevation ($L_w/d_s = 288$) result in higher heat transfer from the surface, compared to the lower water intake elevation. However, the effect of the flow control is larger for $L_w/d_s = 0$. Note that for $L_w/d_s = 0$ the amount of water is smaller that at $L_w/d_s = 288$, and thus it is easier for the synthetic jet to effect the spray.

To gain a better understanding of the effect of the flow control on the heat transfer, spatial distributions of the surface temperature were measured. Surface temperature data were acquired along the two centerlines (perpendicular to one another, along the y- and z-axes). Note that the line of action of the synthetic jets in the flapping mode is along the y-axis.

Fig. 12a–c shows the radial distributions of the change of the surface temperature (with respect to the baseline case) along the y-axis for the three modes of control, and at $Q_a/Q_w = 166$ and at $H/d_s = 35.3$. When four synthetic jets are used (Fig. 12a), the temperature is reduced fairly evenly (13% for the low heat flux and 11% for the higher heat flux, on average). When ramped flapping is used (Fig. 12b), the sides of the heater exhibit larger temperature reduction than the center (up to 11% for the higher heat flux and 25% for the lower heat flux at $r/R = -0.67$), resulting in average temperature reduction of 8% and 20%, respectively, across the central two-thirds of the heater. In the case of on–off flapping mode (Fig. 12c), the cooling of the sides is increased even farther, up to 20.5% for the higher heat flux and 35% for the lower heat flux, with an average temperature reduction of 26% and 16%, respectively. Note that the reduction of the temperature along the z-axis (not shown for brevity) is uniform for all three modes of control.

It appears that at $H/d_s = 23.5$, the flapping motion (i.e., the vectoring of the spray from side-to-side) causes the area

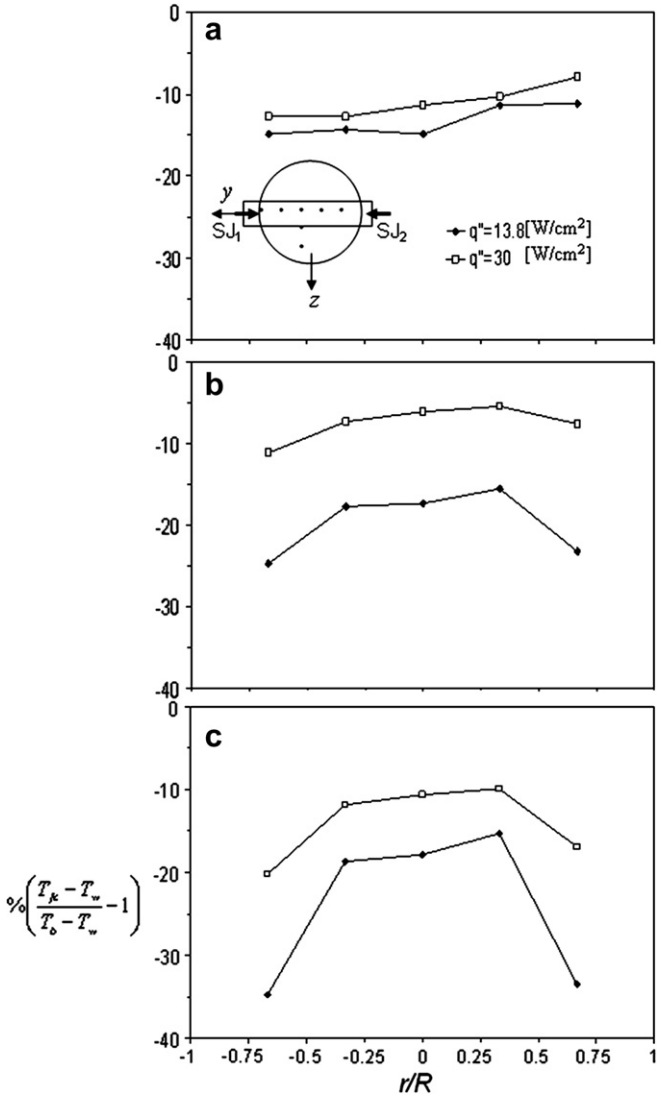

Fig. 12. Radial distributions of the change in temperature compared to the baseline profiles along the y-axis at $H/d_s = 35.3$ and $Q_a/Q_w = 166$ for two heat fluxes. Flow control with four jets (a), ramped flapping (b), and on–off flapping (c).

of high streamwise velocity to move to the very edge of the heater with the fastest droplets impinging on the center of the heater. Moreover, during the flapping process, roughly 40% of the heater is not covered by the spray at all, and is exposed to ambient air, as the spray is vectored away from that area. There is some heat transfer enhancement occurring due to the surface renewal effects, as the horizontal components of velocity due to flapping sweeps the water off the heater to the sides. Note also, that, as was shown in the Shadowgraphy measurements, small droplets move from side-to-side during the flapping motion, which also contributes to the heat transfer enhancement. When all four jets are activated together, the streamwise velocity is reduced as the spray impinges (at $x/d_s = 23.5$), whereas the cross-stream velocity is enhanced (Pavlova et al., 2007, 2008), contributing to a radially outward motion of droplets on the heater after impingement, causing surface

renewal. In addition, droplet size distribution (at this location) remains largely unchanged from the baseline case while velocity RMS is increased.

At $H/d_s = 35.3$, however, the situation is different. Here, the vectoring due to flapping still provides the surface renewal effects, which contribute to better cooling. The vectoring itself moves the portion of high velocity to the edge of the heater, resulting in drastic cooling of the edges, compared to the rest of the heater surface, whereas the spray widens due to vectoring. The widening of the spray keeps the side of the heater (from which the spray is vectored) covered by the spray, such that a very small portion of the heater edge is exposed to the ambient. Ramped flapping reduces the amount of time the spray is at either side and does not provide the horizontal sudden side-to-side motion. When four jets are activated, a horizontal velocity component is imparted to the impinging droplets, aiding in surface renewal, but the effect is not nearly as large as that of ramped and on–off flapping.

In the case of $H/d_s = 47$, the flapping of the spray results moving the high velocity portion of the spray completely off the heater, with the heater still being fully covered by spray droplets. However, the horizontal velocity, imparted to the droplets, removes heated fluid off the surface for better cooling.

When Q_a is the same, but the water intake elevation is decreased, as in Fig. 11, the spray has a very similar velocity profile to that of $Q_a/Q_w = 166$ for the baseline spray (not shown). However, under the influence of a synthetic jet of the same strength, the spray vectors farther away from the synthetic jet (with a slightly lower centerline velocity). The flapping motion causes a portion of the heater (on the opposite side of the vectored spray) to be exposed to the ambient air. Thus, the extra cooling of the heater sides alternates with no spray coverage at all.

4. Conclusions

The effect of active flow control, using synthetic jet actuators, on a water spray and its cooling performance enhancement in the non-boiling regime was investigated experimentally. When a single synthetic jet was activated, it resulted in vectoring of the spray away from the jet, where the vectoring angle was larger for higher momentum coefficients. In addition, the spreading of the spray, in the plane along the synthetic jet, was significantly enhanced, whereas the effect was small in the perpendicular plane. Activation of the synthetic jet also increases the velocity RMS levels throughout the spray flow field. Using two opposing synthetic jets, driven with a ramped function or an on–off mode, resulted in a sweeping of the spray from one side to the other. On–off flapping from side-to-side using two opposing jets was also used by using a step function. Detailed measurements, using Shadowgraphy, showed that the activation of the synthetic jet cause re-distribution of the spray droplets due to the direct impact of the jet onto the spray.

Temperature measurements were performed to assess the effects of active flow control of the spray on the heat transfer from the surface. Three modes of flow control were used, including the activation of four jets, gradual sweeping motion, and activation of two opposing jets in an alternating fashion. Some heat transfer improvements were achieved with flow control, where the mode of flow control, together with spray properties and the distance between the spray and the hot surface play an important role in cooling enhancement. While the heat transfer enhancement is modest and is at lower heat fluxes in the non-boiling regime, it does demonstrate the potential of using active flow control of the spray with synthetic jets and invites further exploration of the technique.

References

Bachalo, W.D., Bachalo, E.J., Hanscom, J.M., Sankar, S.V., 1993. An Investigation of Spray Interactions with Large-Scale Eddies. AIAA paper 930696.

Benajes, J., Payri, R., Molina, S., Soare, V., 2005. Investigation of the influence of injection rate shaping on the spray characteristics in a diesel common rail system equipped with a piston amplifier. J. Fluids Eng. 127, 1102–1110.

Camci, C., Herr, F., 2002. Forced convection heat transfer enhancement using a self-oscillating impinging planar jet. J. Heat Transfer 124, 770–782.

Chen, R.-H., Chow, L.C., Navedo, J.E., 2002. Effects of spray characteristics on critical heat flux in subcooled water spray cooling. Int. J. Heat Mass Transfer 45, 4033–4043.

Chen, R.-H., Chow, L.C., Navedo, J.E., 2004. Optimal spray characteristics in water spray cooling. Int. J. Heat Mass Transfer 47, 5095–5099.

Cossali, G.E., 2001. An integral model for gas entrainment into full cone sprays. J. Fluid Mech. 439, 353–366.

Dubey, R.K., Black, D.L., McQuay, M.Q., Carvalho Jr., J.A., 1997. The effect of acoustics on an ethanol spray flame in a propane-fired pulse combustor. Combust. Flame 110, 25–39.

Estes, K.A., Mudawar, I., 1995a. Comparison of two-phase electronic cooling using free jets and sprays. J. Electron. Packaging 117, 323–332.

Estes, K.A., Mudawar, I., 1995b. Correlation of Sauter mean diameter and critical heat flux for spray cooling of small surfaces. Int. J. Heat Mass Transfer 38, 2985–2996.

Fabbri, M., Jiang, S., Dhir, V., 2003. Comparative Study and Multiple Micro Jets Cooling for High Power Density Electronic Applications. IMECE paper 2003-42325.

Faeth, G.M., Hsiang, L.-P., Wu, P.-K., 1995. Structure and breakup properties of sprays. Int. J. Multiphase Flow 21, 99–127.

Farooq, M., Balachandar, R., Wulfsohn, D., Wolf, T.M., 2001. Agricultural sprays in cross-flow and drift. J. Agr. Eng. Res 78, 347–358.

Gad-el-Hak, M., 2000. Flow Control: Passive, Active, and Reactive Flow Management. Cambridge University Press.

Ghodbane, M., Holman, J.P., 1991. Experimental study of spray cooling with Freon-113. Int. J. Heat Mass Transfer 34, 1163–1174.

Ghosh, S., Hunt, J.C.R., 1998. Spray jets in a cross-flow. J. Fluid Mech. 365, 109–136.

Giles, D.K., Young, B.W., Alexander, P.R., French, H.M., 1995. Intermittent control of liquid flow from fan nozzles in concurrent air streams: wind tunnel studies of droplet size effects. J. Agr. Eng. Res 62, 77–84.

Glezer, A., Amitay, M., 2002. Synthetic jets. Annu. Rev. Fluid Mech., 34.

Hardalupas, Y., Horender, S., 2001. Phase Doppler anemometer for measurements of deterministic spray unsteadiness. Part. Sys. Charact. 18, 205–215.

Hsieh, C.-C., Yao, S-C., 2006. Evaporative heat transfer characteristics of a water spray on micro-structured silicon surfaces. Int. J. Heat Mass Transfer 49, 962–974.

Jia, W., Qiu, H.-H., 2003. Experimental investigation of droplet dynamics and heat transfer in spray cooling. Exp. Therm. Fluid Sci. 27, 829–838.

Kim, J.H., You, S.M., Choi, S.U.S., 2004. Evaporative spray cooling of plain and microporous coated surfaces. Int. J. Heat Mass Transfer 47, 3307–3315.

Kline, S.J., McClintock, F.A., 1953. Describing uncertainties in single sample experiments. Mech. Eng. 75, 3–8.

Lefebvre, A.H., 1989. Atomization and Sprays. Hemisphere Publishing Corporations, 1–417.

Miller, M.F., McManus, K.R., Allen, M.G., 2000. An Aerodynamic Control System for Modifying Fuel Spray Distributions. AIAA Paper 2000-0192.

Mudawar, I., Estes, K.A., 1996. Optimizing and prediction CHF in spray cooling of a square surface. Trans. ASME 118, 672–679.

Navedo, J., 2000. Parametric Effects of Spray Characteristics on Spray Cooling Heat Transfer. Ph.D. dissertation, University of Central Florida.

Oliphant, K., Webb, B.W., McQuay, M.Q., 1998. An experimental comparison of liquid jet array and spray impingement cooling in the non-boiling regime. Exp. Therm. Fluid Sci. 18, 1–10.

Panao, M.R.O., Moreira, A.L.N., 2005. Thermo- and fluid dynamics characterization of spray cooling with pulsed sprays. Exp. Therm. Fluid Sci. 30, 79–96.

Pavlova, A., Otani, K., Amitay, M., 2007. Active Flow Control of Sprays with Synthetic Jets. AIAA paper 2007-322.

Pavlova, A., Otani, K., Amitay, M., 2008. Active flow control of sprays using a single synthetic jet. Int. J. Heat Fluid Flow 29, 131–148.

Pothos, S., 2002. Control of Particles and Turbulence Using a Piezoelectric Actuator. Doctoral Thesis, University of Minnesota.

Pothos, S., Longmire, E.K., 2002. Control of a particle-laden jet using a piezo-electric actuator. In: 11th International Symposium on Applications of Laser Techniques to Fluid Mechanics, Lisbon, July 2002.

Pimentel, R.G., deChamplain, A., Kretschmer, D., Stowe, R.A., Harris, P.G., 2006. Generalized Formulation for Droplet Size Distribution in a Spray. AIAA paper 2006-4918.

Ramanaryanan, B., Sujith, R.I., Chakravarthy, S.R., 2003. Characterization of an Acoustically Self-Excited Combustor for Spray Evaporation. AIAA paper 2003-502.

Shiina, K., Nakamura, S., Narita, K., 2000. Cooling characteristics of an impinging spray jet which forms an ellipsoidal liquid film. Heat Trans. – Asian Res. 29 (4), 280–299.

Sirignano, W.A., 1999. Fluid Dynamics and Transport of Droplets and Sprays. Cambridge University Press.

Smith, B.L., Glezer, A., 1998. The formation and evolution of synthetic jets. Phys. Fluids 31, 2281–2297.

Sujith, R.I., 2003. An Experimental Investigation of Interaction of Sprays with Acoustic Fields using PIV. AIAA paper 2003-0318.

Sujith, R.I., 2005. An experimental investigation of interaction of sprays with acoustic fields. Exp. Fluids 38, 576–587.

Sujith, R.I., Walherr, G.A., Jagoda, J.I., Zinn, B.T., 1997. An experimental investigation of the behavior of droplets in axial acoustic fields. J. Vibrat. Acoust. 119, 285–292.

Tszeng, T.C., Saraf, V., 2003. A study of fin effect in the measurement of temperature using surface-mounted thermocouples. J. Heat Transfer 125, 926–935.

Wang, D., Ganji, A.R., Sipperley, C.M., Edwards, C.F., 1999. Effects of Nozzle Geometry and Ambient Pressure on the Characteristics of a Modulated Spray. AIAA paper 99-0366.

Zhu, M., Dowling, A.P., Bray, K.N.C., 2002. Forced oscillations in combustors with spray atomizers. J. Eng. Gas Turb. Power 124, 20–30.